Fragmentation detection via track-to-track association of optical observations

Alejandro Pastor
GMV, apastor@gmv.com
Guillermo Escribano
Universidad Carlos III de Madrid, guescrib@ing.uc3m.es
Manuel Sanjurjo-Rivo
Universidad Carlos III de Madrid, manuel.sanjurjo@uc3m.es
Diego Escobar
GMV, descobar@gmv.com

Abstract

In-orbit fragmentations are the main source of space debris. Such events have taken place just some years after the launch of the first artificial satellite and are the sources of most of the current space debris population. During the first stage after a fragmentation event, the states of the fragments are expected to be very similar since not enough time has yet passed since the event for the fragments to separate. Fragments have not spread along the orbit, and it might not be possible to distinguish individual objects, reason why they are usually referred to as debris cloud. Only once the observable state separation of the fragments is greater than the one resulting from the expected sensor noise and dynamical model error, it is possible to start the identification, orbit determination (i.e., catalog build-up) and subsequent update (i.e., catalog maintenance) of the break-up fragments. Then, it is possible to use track-to-track association algorithms to solve the association problem arising from a fragmentation event. To do so, associations of tracks, or hypotheses, are generated, scored and pruned in real-time using several complexity reduction techniques. Fragments are identified, i.e.: hypotheses promoted, as enough sensing data is associated and the resulting orbit estimation is accurate enough to enable subsequent correlation of future tracks via track-to-orbit correlation methods. The use of this methodology during catalog build-up and maintenance operations would enable the automatic detection of fragments and reduce the detection time, which nowadays may take from weeks up to months. To study the performance of the track-to-track association methodology, an explosion of a Geostationary Earth Orbit (GEO) satellite has been simulated, as well as observations from the fragments with a Space Surveillance and Tracking (SST) optical sensor network of five telescopes. Then, track-to-track association is used to detect the fragments from the simulated observations and the resulting association metrics are discussed and particular cases are used to unveil the main challenges of the fragmentation detection problem.

1. INTRODUCTION

In June 29th, 1961, the Thor Able Star second stage exploded, two hours after separating from the Transit 4-A satellite. This event happened less than four years after the first launch of an artificial satellite, Sputnik 1, and generated a number of trackable objects three times greater than the number of known satellites at that time in orbit. Since then, in-orbit fragmentations have been the most dominant source of space debris in the millimeter to decimeter size range. This is particularly critical for space safety, since objects in the upper part of this size range (centimeter to decimeter) are associated to the highest risk, given the current limits of shielding technology [1].

The 18th Space Control Squadron (SPCS) maintains one of the most complete and publicly available catalogs of resident space objects. It is published on Space-Track and contains more than 22,000 objects of which more than half are classified as fragmentation debris. The typical minimum size object that the 18th SPCS can currently track is around 10 centimeters in low orbits and 1 meter at Geostationary Earth Orbit (GEO), although these thresholds are expected to fall in the coming years due to the improvement of the Space Surveillance and Tracking (SST) sensor technology. The estimated number of objects between 1 and 10 cm size is not lower than 500,000 and thus we expect an important increase in complexity of catalog build-up and maintenance activities.

National Aeronautics and Space Administration (NASA) has been publishing a report on the history of on-orbit satellite fragmentations since 1984. The 15th edition [2], the most recent one, was published in 2018 and includes very valuable data about satellite break-ups up to 4 July 2018. Figure 1 shows the number of cataloged orbits and fragments still in-orbit from identified satellite break-up events in [2]. The two most recent peaks correspond to the Fengyun-1C anti-satellite test (2007) and the COSMOS 2251 and Iridium 33 collision (2009).

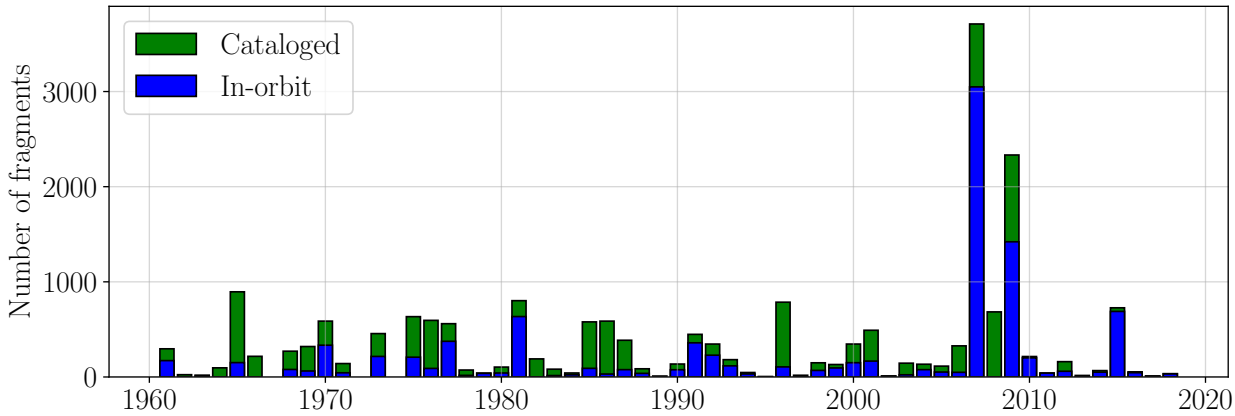

Figure 1: Number of cataloged (green) and in-orbit (blue) fragments from identified satellite break-up events per year according to [2] (from 1961 to 2018).

There are two main problems related to fragmentation events: 1) the detection of the fragments and first estimation of the orbits using observations from SST sensors and 2) the analysis of the fragmentation event using orbital data. This paper tackles the first problem and leaves the second one for future works.

Regarding the first problem, the detection of fragments after a collision between Highly Elliptical Orbit (HEO) and Low Earth Orbit (LEO) satellites with ground-based optical sensors is analysed in [3]. The problematic of both large and small mean motion spreading of the fragments is discussed in [4] and [5], respectively. Survey and tracking strategies must be optimized to maximize the number of detections and minimize the number of lost fragments [6]. Besides, magnitude measurements have been also used to identify fragments from a common break-up event [7]. Since the second problem involves the availability of orbits from the fragments, it is usually tackled using Two Line Elements (TLEs) (from Space-Track [8]) [9, 10, 11]. Ephemerides from the JSC Vimpel catalog [12] have also been successfully used for a-posteri analyses [13]. When available, the uncertainty in the orbits can be used to improve the estimation of the blast point [14]. Moreover, particular orbit similarity metrics have been conceived for the correlation of cataloged debris fragments and parent bodies [15].

This paper presents the application of our track-to-track association methodology [16] to the problem of detecting fragments from a break-up event. This methodology was conceived for operational survey scenarios and therefore it is relevant to investigate its performance in the presence of fragmentation clouds, given their relevance during catalog build-up.

This paper is organized as follows. In Section 2, we present the fragmentation simulation, observation simulation and track-to-track association processes. In Section 3, we provide and discuss the results obtained evaluating the performance of the track-to-track association methodology and highlighting the main drivers of the association. Finally, in Section 4, we summarize and discuss the conclusions and future work of this preliminary study.

2. METHODOLOGY

2.1 Fragmentation simulation

The NASA Standard Breakup Model (SBM) [17] has been used to simulate the size, area-to-mass ratio (A/M) and relative velocity increment (ΔV) of the fragments originated from an in-orbit fragmentation event of a 36º West GEO satellite. The initial state of the parent object has been taken from a TLE published on Space-Track on 2019-12-31T22:20:17 [8] and the physical properties from [18]. An in-orbit fragmentation event involving 200 fragments has been simulated by adjusting the explosion scaling factor, included in the NASA SBM [17]. The details of the simulated in-orbit fragmentation event are compiled in Table 1.

Table 1: Fragmentation simulation details.

Parent object	
Semi-major axis (km)	42,165.12
Eccentricity	0.0001
Inclination (deg)	0.0097
m (kg)	1700
A/m (m^2/kg)	0.0034

Fragmentation event	
Type	Explosion
Minimum fragment size (m)	1.0
Explosion scaling factor	34.9
Number of fragments	200

The fragmentation is simulated as an impulsive velocity increase, ΔV, that is added to the state of the parent object. The distribution of the ΔV in the RIC frame (radial, in-track and cross-track directions) is presented in Figure 2, where the histogram is presented along with the Cummulative Distribution Function (CDF), as a result of the NASA SBM.

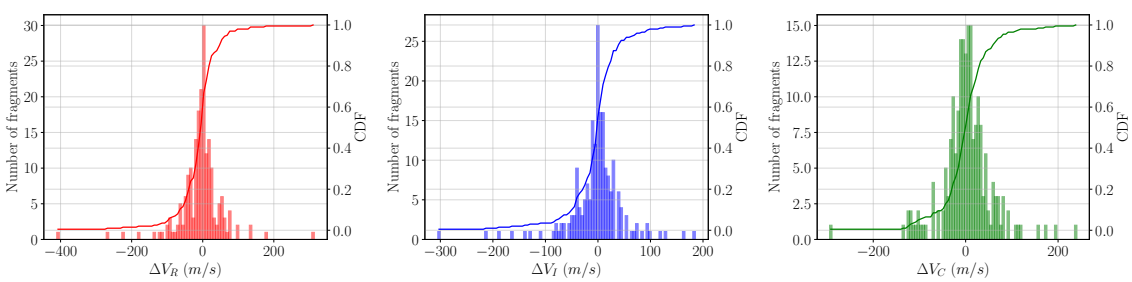

Figure 2: Distribution of the simulated ΔV.

The Gabbard diagram of the simulated fragmentation is show in Figure 3, where the dashed lines represent the perigee, apogee and orbital period of the parent object. Since the parent object is describing a nearly circular orbit, there is a clear intersection point (corresponding to the orbit of the parent object, with nearly same perigee and apogee heights) and the in-track and along-track components of the velocity are almost the same. Accordingly, ΔV_I is directly related with changes in the orbital energy and thus, in the orbital period. Therefore, the points lying to the right of the vertical dotted line represent fragments with posigrade impulses ($\Delta V_I > 0$), while those lying to the left represent fragments with retrograde impulses ($\Delta V_I < 0$). Besides, due to the nearly circular orbit, the typical inclined X [19] is present. However, since the impulse has also some radial component (ΔV_R), there are points lying outside the two main straight lines (above apogee and below preigee). Moreover, the angle between the two intersecting lines (slopes of the apogee and perigee lines) is related to the true anomaly of the parent object at the fragmentation epoch. Note the Gabbard diagram does not depend on ΔV_C since it is a velocity component out of the orbital plane, and not related to apogee, perigee nor orbital period.

The distribution of the mass and size of the simulated fragments is presented in Figure 4. Note that we have set a minimum fragment size of 1 m to ensure telescopes are able to observe the fragments, although we plan to decrease this number in the future. However, this should only impact the Solar Radiation Pressure (SRP) from the dynamical point of view.

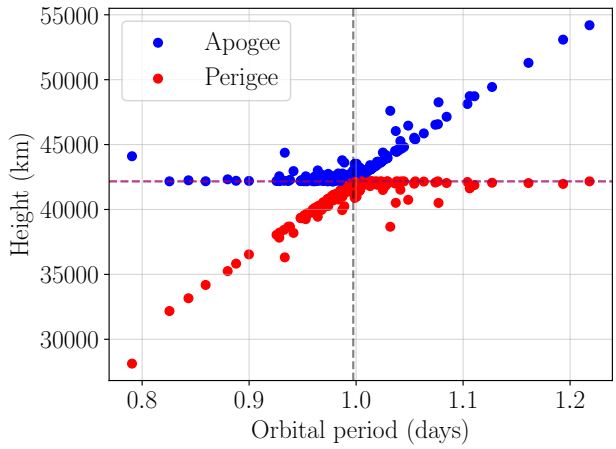

Figure 3: Gabbard diagram of the simulated in-orbit fragmentation event.

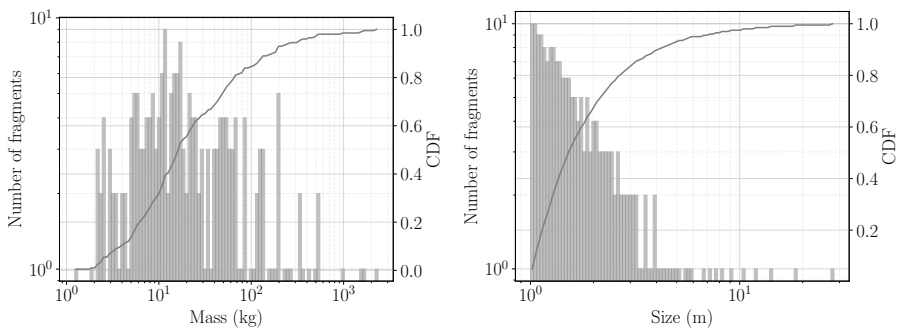

Figure 4: Distribution of the mass and size of the simulated fragments.

2.2 Observation simulation

The orbits of the fragments have been propagated one month forward in time with a high-fidelity dynamical model [1]. Figure 5 shows the evolution of the standard deviation of the difference between the longitude of the fragments and the longitude of the parent object, if still in-orbit, σ_λ, along with the longitude distributions after 1, 5 and 15 days. It represents the dispersion in longitude of the fragments, which exhibits a quadratic growth during the first two weeks, until the fragments fill the longitude plane. Once the trajectories of the fragments are available, observations are simulated for a ground-based optical network consisting of 5 telescopes located in Azores, mainland Spain, Réunion, Chile and New Zealand (see Figure 6, left). The five sensors are modeled all in the same manner. The details of the observation simulation are compiled in Table 2.

The survey strategy simulated for all sensors consists of a typical leak proof strategy with two vertical barriers during each night. The strategy tries to observe each fragment twice per night by considering two declination barriers in the right ascension and declination plane. First, the target declination is obtained by maximizing the number of objects observed from a background population. Then, for each target declination, the right ascension is optimized so that both the brightness and survey time are maximized while taking into account typical constraints (night period, elevation, galactic plane, Moon, Sun illumination and pointing phase angle).

The simulated observations are packed in tracks, sets of observations taken by a single sensor during certain period of time of continuous observation of an object. There are a total of 10,901 tracks distributed along the first month after the fragmentation. See the share between sensors in Figure 6, right. The distribution of the duration of the simulated tracks, i.e. time between the last and first observation, is presented in Figure 7.

[1] Animations showing the trajectories of the fragments are available at https://gmvdrive.gmv.com/index.php/s/8pMZBDBHLi6BDRB (first week), and https://gmvdrive.gmv.com/index.php/s/n6Yjo9A4rigf9y7 (fourth week).

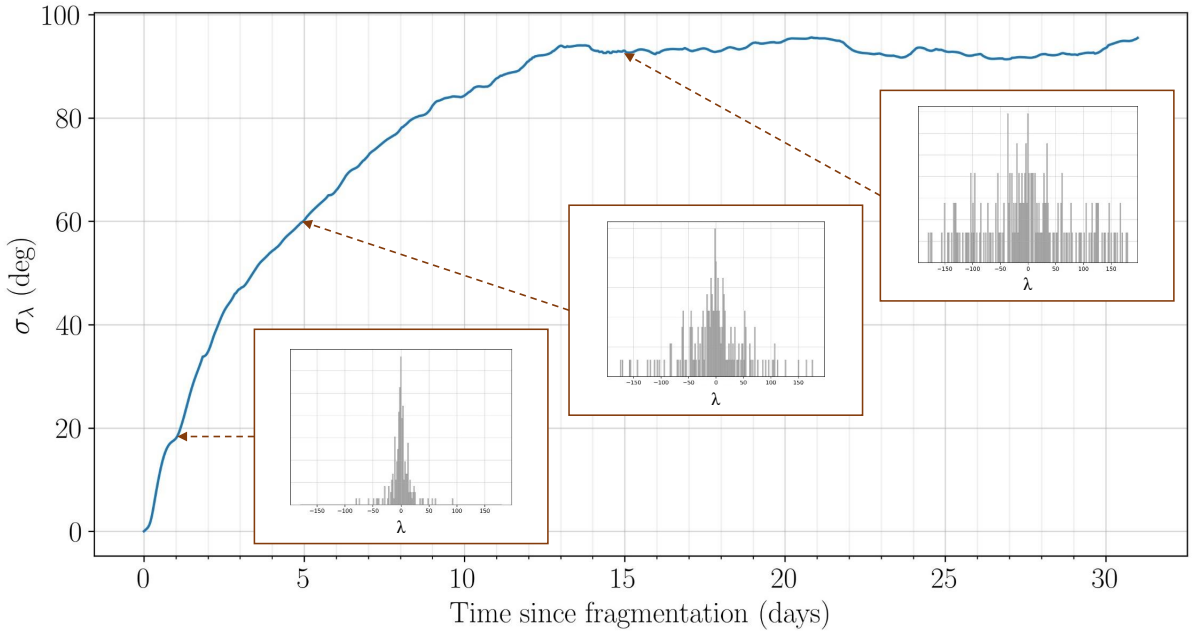

Figure 5: Evolution of σ_λ along time after fragmentation.

Table 2: Observation simulation details.

Propagation model	
Gravity field	EIGEN-6S2 100x100
Third bodies	Sun + Moon (JPL DE405)
SRP	Cannonball model
Propagation time (days)	31.0

Sensor model	
Field of view	Pyramidal: 4x4 deg
Cut-off elevation (deg)	15.0
Measurement #1	Right ascension
Measurement #2	Declination
1-sigma noise (arcsec)	1.0
Observation spacing (s)	60.0

2.3 Track association

Once the simulated observations are obtained, the track-to track association methodology presented in [16] has been used to automatically group tracks so that they belong to the same fragments. In this framework, a hypothesis represents an association of certain number of tracks and hypotheses are generated, scored, pruned and promoted as tracks are received. In line with [16, 20], only hypotheses of four tracks are promoted, if the corresponding figure of merit, d, is below the threshold $d_{max} = 1.5$. Besides, the dynamical model used for the track association is a semi-analytical propagator, different from the one used for the propagation of the fragments. Once a hypothesis has been promoted, an Orbit Determination (OD) is performed to initialize the orbit of the new object in the catalog. During the generation of hypotheses of three and four tracks, a time span between associated tracks of at least 0.25 times the estimated orbital period is required, for the purpose of avoiding orbit observability problems. Finally, a simulated track-to-orbit process has been added to the track association algorithm. Tracks from already detected fragments (promoted hypotheses) are skipped, since they are assumed to be correlated with the orbits of the detected fragments.

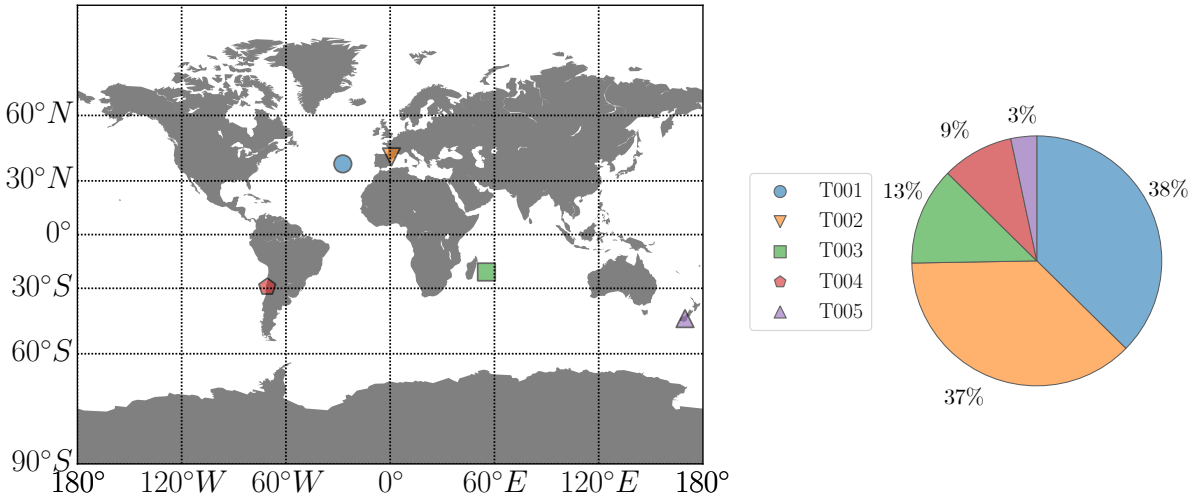

Figure 6: Location of the ground-based optical sensor network (left) and track share of each sensor (right).

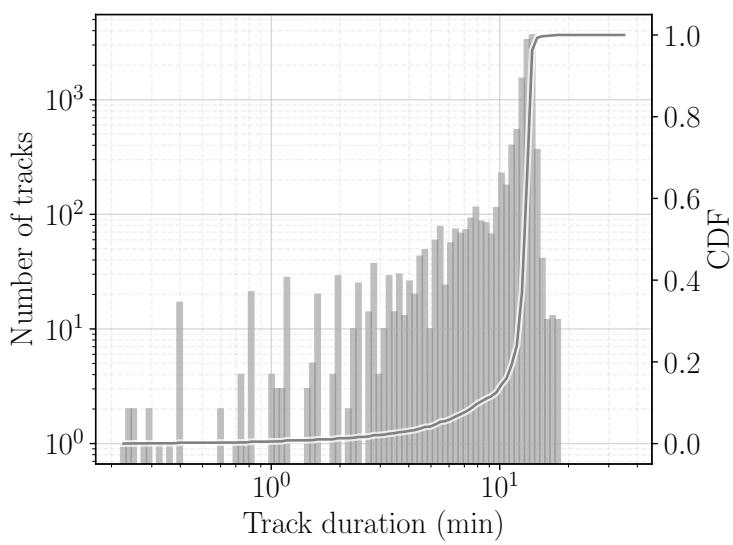

Figure 7: Distribution of the duration of the simulated tracks.

3. RESULTS

The number of hypotheses at the end of the simulation is compiled in Table 3 where N denotes the number of associated tracks. Hypotheses are classified as *promoted* or *under-analysis* depending on whether the associations have been promoted or not (recall that four tracks are required to promote a hypothesis). The *validity* of the hypotheses refer to the fragment matching of the associated tracks since the originating fragment is known in this simulated scenario. Note that, due to the simulated track-to-orbit correlation performed after the detection of each fragment (see Section 2.3), each promoted hypothesis represents one fragment detection. Therefore, 199 fragments (i.e. 99.5% of the total 200 simulated fragments) are detected, true positives, while there is only one false promoted hypothesis, false positive.

Table 3: Number of hypotheses at the end of the simulation.

Hypotheses	Validity	$N=1$	$N=2$	$N=3$	$N=4$
Under-analysis	True	627	803	229	1
	False	N/A	101,266	34,119	4,475
Promoted	True	0	0	0	199
	False	0	0	0	1

Figure 8 shows the distribution of the figure of merit, d, of the hypotheses of four tracks (last column of Table 3) as a function of the semi-major axis, a, and eccentricity, e, of the corresponding fragments. Besides, Figure 9 presents the distribution of the figure of merit of the same hypotheses but as a function of the time span between first and last associated tracks, $\Delta t_{1,4}$. True positives, false positives, false negatives and true negatives are depicted in green circles, red crosses, purple triangles up and blue triangles down, respectively. There is a clear separation between true positives and and true negatives, which suggests the figure of merit proposed in previous works can indeed be used also in fragmentation events. Moreover, there are no signs of degradation of the figure of merit with respect to the semi-major axis nor eccentricity. The distributions of hypotheses are consistent with the fragment population density. Regarding the $\Delta t_{1,4}$, there are tracks separated even more than 15 days that can be associated.

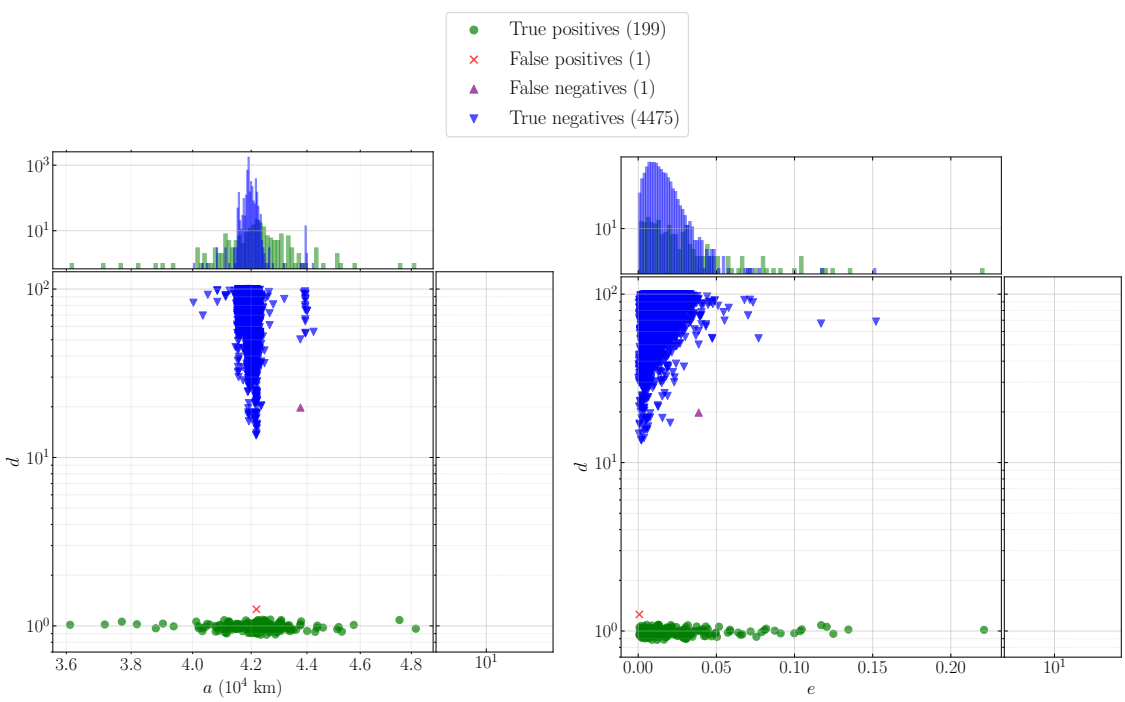

Figure 8: Distribution of the figure of merit of the hypotheses of four tracks as a function of the semi-major axis (left) and eccentricity (right) of the corresponding orbit.

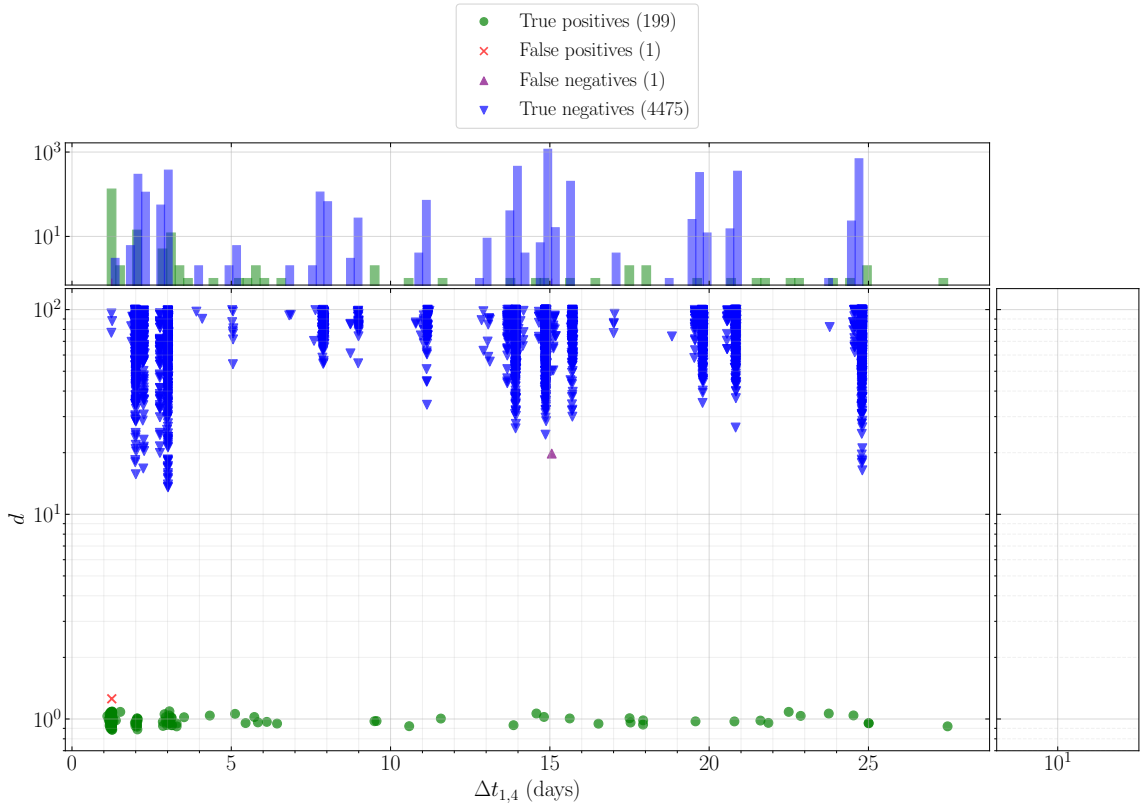

Figure 9: Distribution of the figure of merit of the hypotheses of four tracks as a function of the time span between first and last associated tracks.

The false promoted hypothesis of four tracks corresponds to the association of: 1) track from T001 at day #1 23:20 from fragment #6, 2) track from T001 at day #2 05:16 again from fragment #6, 3) track from T002 at day #2 23:14 from fragment #39, and 4) track from T002 at day #3 05:31 again from fragment #39. These two fragments have a similar orbit, the velocity increase of the fragment #4 in the RIC frame is $\Delta V = [2.319, -0.251, 2.001]\, m/s$ and that of the fragment #37 is $\Delta V = [2.310, 0.176, 1.888]\, m/s$. The ΔV_R and ΔV_C are close and the ΔV_I is relatively small, so it is expected that during the time span between first and last associated tracks: less than three days, these two fragments have not yet been separated enough to be distinguished [2]. However, this hypothesis has the largest figure of merit ($d = 1.26$) of all the promoted hypothesis and it is close to the threshold ($d_{max} = 1.3$). Requiring the associated tracks to be separated longer periods of time, and further from the event, would allow to avoid this false positive, although it may also increase the detection time.

The only true hypothesis of four tracks still under-analysis (false negatives) of four tracks correspond to the association of: 1) track from T001 at day #2 00:40, 2) track from T002 at day #16 00:24, 3) track from T002 at day #16 20:10, and 4) track from T002 at day #17 02:05, all from fragment #102. The time span between the first and last associated tracks is 15 days, which may be too long taking into account the mismatch between the dynamical models used for propagation and association. In this case, $d = 19.8$, far from d_{max}, and therefore the hypothesis is not promoted. Noteworthy, this fragment was detected (i.e. there is a promoted hypothesis of tracks of this fragment) by associating a different set of posterior tracks.

Figure 10 and Figure 11 show the distribution of the figure of merit of the hypotheses of two and three tracks as a function of the time span between first and last associated tracks, $\Delta t_{1,2}$ and $\Delta t_{1,3}$, respectively. Regarding the associations of two tracks (Figure 10), there is a noticeable overlap in the figure of merit of false and true negatives. There is still not enough data to make a hard decision (i.e., promote hypotheses). When hypotheses of three tracks (Figure 11) are considered, the resulting separation between false and true negatives becomes greater. Nevertheless,

[2] A video showing the trajectory of these two fragments is available at https://gmvdrive.gmv.com/index.php/s/WMXFFefpBbzHP6Z.

there is still certain ambiguity not present in the distribution of hypotheses of four tracks (Figure 9). Note that only hypotheses of four tracks have been considered for promotion, but it could be possible to promote also hypotheses of three tracks under particular conditions. However, this must be further investigated to avoid low accuracy orbit initialization during catalog build-up.

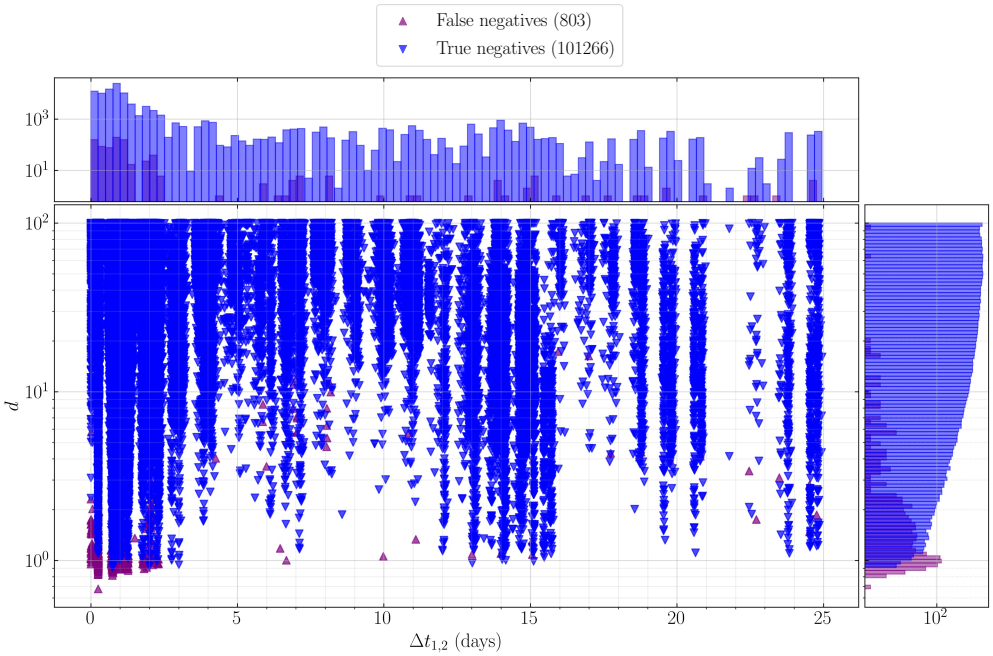

Figure 10: Distribution of the figure of merit of the hypotheses of two tracks as a function of the time span between first and last associated tracks.

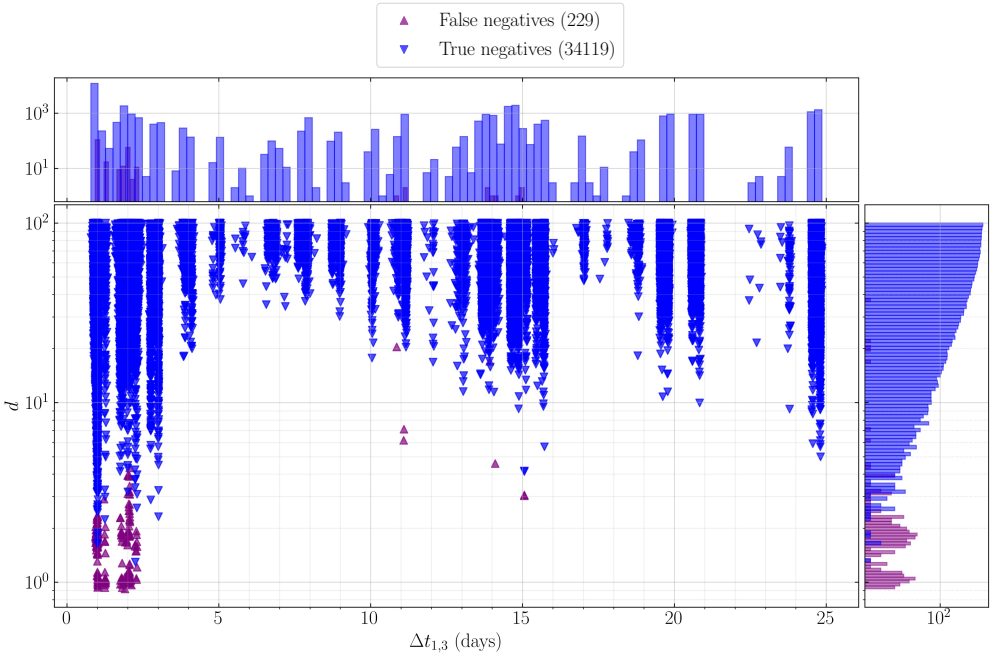

Figure 11: Distribution of the figure of merit of the hypotheses of three tracks as a function of the time span between first and last associated tracks.

In terms of objects, Figure 12 shows the semi-major axis and eccentricity of every detected (199) and undetected (1) fragment. The latter, which represents a false negative in terms of detected objects, has an eccentricity of 0.1 and although a total of 8 tracks from five sensors are received along the simulation, they correspond to similar points in the orbit (in terms of true anomaly, ν). Seven of these tracks correspond to $\nu \in (2.25, 4.89)^\circ$ and the remaining one to $\nu = -21.25^\circ$. This is a challenging detection due to the combination of bad observability and eccentricity of the orbit. Given that this missed detection is mainly related to the estimation counterpart of the track association, an isolated scenario with these eight tracks and the recent improvement in the Initial Orbit Determination (IOD) algorithm discussed in [21] and detailed in [22], allows to the promotion of a hypothesis of four tracks (the one related to $\nu = -21.25^\circ$, among them) with a figure of merit of $d = 0.94$.

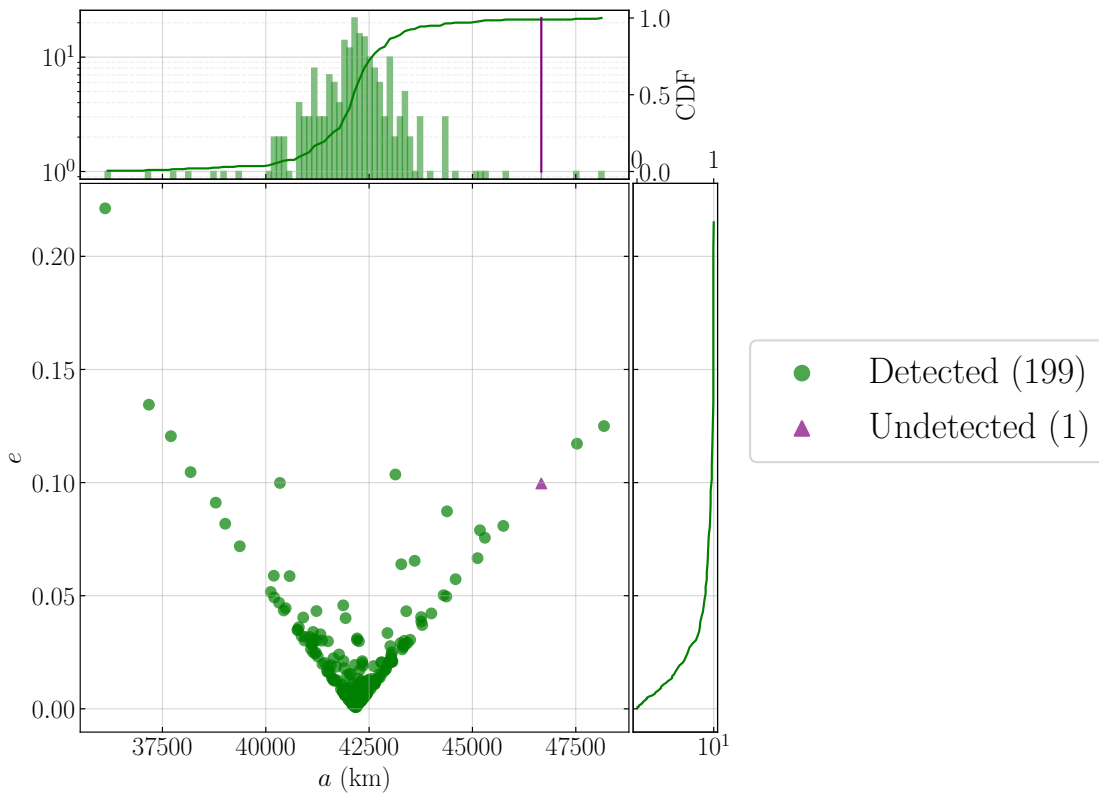

Figure 12: Distribution of the semi-major axis and eccentricity of detected and undetected fragments.

The evolution of the number of detected fragments (promoted hypotheses) and non-promoted hypotheses along the time since the fragmentation event is depicted in Figure 13. The number of non-promoted hypotheses starts growing soon due to the generation of associations of two and three tracks but stabilizes once most of the fragments have been detected due to the pruning of incompatible hypotheses. Besides, it takes one and a half days (two nights) to start detecting fragments, mainly due to the time span constraint (0.25 times the orbital period for associations of three and four tracks), which is directly related to orbit observability. Two and three days after the fragmentation more than 130 and almost 145 fragments have been detected, respectively. Then, from the fourth day (164 detections), the number of detections increases up to day 25th day (198 detections) and finally 28th day (199 detections).

4. CONCLUSIONS AND FUTURE WORK

This paper has presented a simulated scenario of a GEO explosion causing an in-orbit fragmentation event involving 200 fragments being observed by a sensor network of five telescopes. The details of the fragmentation, simulated according to NASA SBM [17], have been discussed, with particular emphasis on the Gabbard diagram and the impulsive ΔV making the fragments move away from the trajectory of the parent object. Besides, the method for simulating the observations has been described, including the survey strategy. The track-to-track association

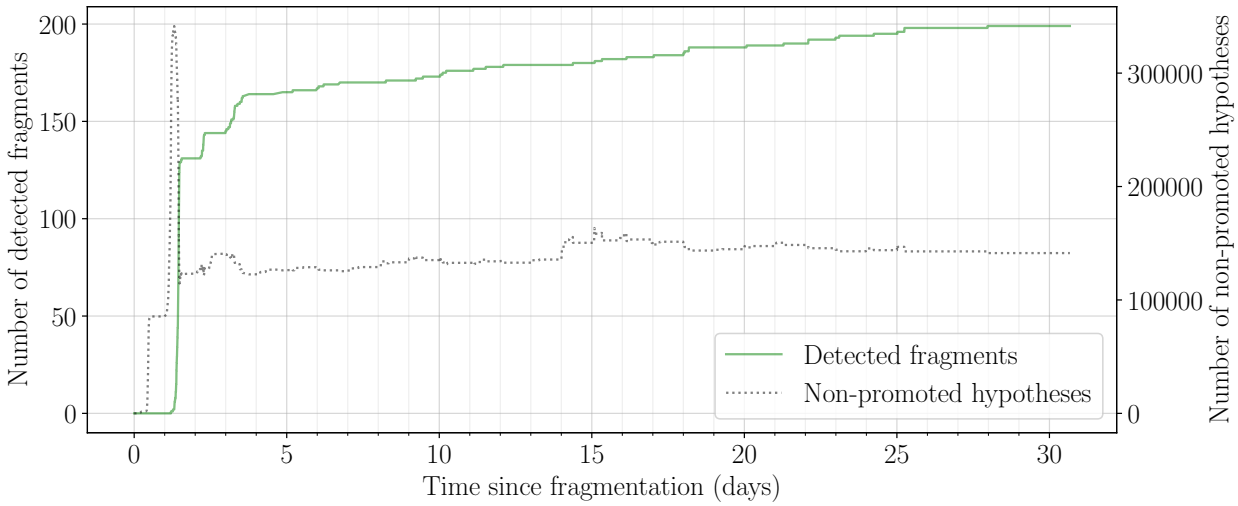

Figure 13: Evolution of the number of detected fragments and non-promoted hypotheses along the time since fragmentation.

methodology presented in [16] has been applied for the detection of fragments and the results suggest the suitability of the approach. The methodology is able to detect most (199) of the fragments, thus remaining only one undetected, while promoting only one false hypothesis (false positive). The figure of merit is able to isolate most of the true hypotheses from the false ones even when the tracks are separated more than two weeks. Despite of this, most of the fragments are detected within the first days after the fragmentation, which is crucial in real scenarios to perform an early catalog build-up and maintenance. In fact, as expected, the first days after the fragmentation are the most challenging ones from the track association perspective, since track-to-orbit is not possible until fragments are cataloged and also because the objects still remain on the fragmentation cloud, i.e. they have not yet been spread along different orbits. Moreover, the role of the orbit observability in the track association has been also presented. A complete sensor network with stations located around the globe is required to maximize the detection rate, since this leads to higher number of tracks but also to better observability, which is of major interest particularly for fragments describing eccentric objects.

This work is an on-going research project and therefore represents a preliminary study on the application of track-to-track association methodologies to the fragmentation detection problem. Future work will focus on the simulation of the complete cataloging process, thus replacing the track-to-orbit simulator by an actual track-to-orbit correlation algorithm. This would also enable to assess the accuracy of the estimated orbits of the fragments through time, since once the fragment is detected, the next tracks could be correlated and used to improve the maintained orbit via OD. Besides, additional efforts are needed to evaluate explosion and collision events involving higher numbers of fragments, as well collisions, and reduce the size distribution.

ACKNOWLEDGEMENTS

This project has received funding from the “Comunidad de Madrid” under “Ayudas destinadas a la realización de doctorados industriales” program (project IND2017/TIC7700).

Besides, the authors would like to acknowledge the contributions from Alfredo Antón for providing the implementation of the NASA SBM, David Moreno for his support with the sensor survey law, as well as Daniel Sáez, Vlad-Marian Ivanciu and Adrián Rabadán for producing the fragmentation animations.

REFERENCES

[1] H. Klinkrad, Space Debris: Models and Risk Analysis, Springer-Verlag Berlin Heidelberg, 2006. doi:10.1007/3-540-37674-7.

[2] P. Anz-Meador, J. Opiela, D. Shoots, J. Liou, History of on-orbit satellite fragmentations, 15th edition, Tech. Rep. NASA/TM–2018–220037, NASA Orbital Debris Program Office (2018).

[3] R. Crowther, R. Walker, J. Dick, S. Green, J. Marchant, Detectability of satellite fragmentations in highly eccentric orbits, Master's thesis (jan 1995). doi:10.1016/0273-1177(95)98762-d.

[4] C. Saunders, Modelling of the optical observations of a geosynchronous fragmentation event, Acta Astronautica 60 (8-9) (2007) 752–762. doi:10.1016/j.actaastro.2006.07.021.

[5] T. Schildknecht, A. Vananti, E. Cordelli, T. Flohrer, ESA optical surveys to characterize recent fragmentation events in GEO and HEO, in: S. Ryan (Ed.), Advanced Maui Optical and Space Surveillance Technologies Conference, 2019, p. 34.

[6] V. Agapov, A. Lapshin, Survey and follow-up strategies used in operation of ASPOS OKP to gather observation data on GEO, HEO and MEO objects, in: T. Flohrer, R. Jehn, F. Schmitz (Eds.), 1st NEO and Debris Detection Conference, Vol. 8, ESA Space Safety Programme Office, 2019.

[7] G. Zarcone, L. Mariani, M. Rossetti, L. Cimino, S. H. Hossein, F. Piergentili, F. Santoni, F. Curianò, Optical observations for energetic characterization of in-orbit explosion: the FREGAT-SB case, in: T. Flohrer, S. Lemmens, F. Schmitz (Eds.), 8th European Conference on Space Debris, Vol. 8, ESA Space Debris Office, 2021.

[8] Combined Force Space Component Command, Space-Track (Accessed Aug 2021).
URL https://space-track.org

[9] N. L. Johnson, E. Stansbery, J.-C. Liou, M. Horstman, C. Stokely, D. Whitlock, The characteristics and consequences of the break-up of the Fengyun-1C spacecraft, Acta Astronautica 63 (1-4) (2008) 128–135. doi:10.1016/j.actaastro.2007.12.044.

[10] K. Tetreault, S. D. Ross, K. Schroeder, J. Black, Fragmentation event identification using back propagation with variable ballistic coefficient calculation, in: Advanced Maui Optical and Space Surveillance Technologies Conference, 2018.

[11] A. Muciaccia, Fragmentations in low earth orbit: event detection and parent body identification, Master's thesis, Politecnico di Milano (2021).

[12] JSC "Vimpel Interstate Corporation" and the Keldysh Institute of Applied Mathematics (IAM), JSC Vimpel data portal (Accessed Aug 2021).
URL http://spacedata.vimpel.ru/

[13] P. Ravi, C. Frueh, T. Schildknecht, Investigation of three recent Atlas V Centaur upper stage fragmentation events, in: T. Flohrer, S. Lemmens, F. Schmitz (Eds.), 8th European Conference on Space Debris, Vol. 8, ESA Space Debris Office, 2021.

[14] W. Faber, W. Zaidi, J. Schumacher, Paul, Early blast point determination for large GEO fragmentation events, in: S. Ryan (Ed.), Advanced Maui Optical and Space Surveillance Technologies Conference, 2018, p. 22.

[15] L. Dimare, S. Cicalò, A. Rossi, E. M. Alessi, G. B. Valsecchi, In-orbit fragmentation characterization and parent bodies identification by means of orbital distances, in: First International Orbital Debris Conference, Vol. 2109, 2019, p. 6007.

[16] A. Pastor, D. Escobar, M. Sanjurjo-Rivo, A. Águeda, Object detection methods for optical survey measurements, in: 20th Advanced Maui Optical and Space Surveillance Technologies, 2019.

[17] N. Johnson, P. Krisko, J.-C. Liou, P. Anz-Meador, Nasa's new breakup model of evolve 4.0, Advances in Space Research 28 (9) (2001) 1377–1384. doi:10.1016/s0273-1177(01)00423-9.

[18] H. J. Kramer, SmallGEO (Small Geostationary Satellite Platform) Initiative / Hispasat AG1 Mission / H36W-1 (Accessed Aug 2021).
URL https://directory.eoportal.org/web/eoportal/satellite-missions/s/smallgeo

[19] A. Tan, R. C. Reynolds, Theory of satellite fragmentation in orbit, World Scientific Publishing Co. Pte. Ltd., 2020. doi:10.1142/11506.

[20] K. Hill, C. Sabol, K. T. Alfriend, Comparison of covariance based track association approaches using simulated radar data, The Journal of the Astronautical Sciences 59 (1-2) (2012) 281–300. doi:10.1007/s40295-013-0018-1.

[21] A. Pastor, M. Sanjurjo-Rivo, D. Escobar, Track-to-track association for space object cataloguing with optical survey data, in: 71st International Astronautical Congress, 2020.
[22] A. Pastor, M. Sanjurjo-Rivo, D. Escobar, Initial orbit determination methods for track-to-track association, Advances in Space Research 68 (7) (2021) 2677–2694. doi:10.1016/j.asr.2021.06.042.